Optical Engineering

OpticalEngineering.SPIEDigitalLibrary.org

Effects of misalignments on the modulation transfer function measurement of camera lenses analyzed in optomechanical simulations

Melissa Schenker
Manuel Stavridis
Michael Schulz
Rainer Tutsch

SPIE.

Melissa Schenker, Manuel Stavridis, Michael Schulz, Rainer Tutsch, "Effects of misalignments on the modulation transfer function measurement of camera lenses analyzed in optomechanical simulations," *Opt. Eng.* **59**(3), 034101 (2020), doi: 10.1117/1.OE.59.3.034101

Effects of misalignments on the modulation transfer function measurement of camera lenses analyzed in optomechanical simulations

Melissa Schenker,[a,*] Manuel Stavridis,[b] Michael Schulz,[a] and Rainer Tutsch[c]

[a]Physikalisch-Technische Bundesanstalt, Braunschweig, Germany
[b]Physikalisch-Technische Bundesanstalt, Berlin, Germany
[c]Technische Universität Braunschweig, Institut für Produktionsmesstechnik, Braunschweig, Germany

Abstract. The Physikalisch-Technische Bundesanstalt has developed a reference setup for measuring the modulation transfer function (MTF) of camera lenses with the goal of reaching an expanded measurement uncertainty of 0.01 (coverage probability of 95%) for various measurement configurations. We present optomechanical simulations of the setup behavior, which are used to investigate the influence of the combined mechanical misalignments on the MTF depending on the lens under test. The investigations are carried out as part of Monte Carlo studies for different sample lenses and field heights considering the correlations between the effects of different positioning errors on the MTF measured. The results of the sensitivity analyses have allowed appropriate alignment strategies to be identified that significantly reduce the uncertainty contribution of the positioning errors. By implementing these strategies, the target measurement uncertainty can be achieved for most of the desired measurement configurations. In addition, the comparison of three different sample lenses shows that the MTF sensitivity to misalignments strongly depends on the characteristics of the lens to be measured. [DOI: 10.1117/1.OE.59.3.034101]

Keywords: optical metrology; modulation transfer function; camera lenses; imaging performance; virtual experiments.

Paper 191576 received Nov. 7, 2019; accepted for publication Feb. 11, 2020; published online Mar. 3, 2020.

1 Introduction

Recent developments in the use of camera lenses—e.g., in smartphones, professional cine cameras, or cameras used in advanced driver-assistance systems—necessitate high-precision quality control procedures to ensure high performance, cost-effective production, and compliance with safety aspects.[1–3] Since the theory of optical transfer function was described and the first measuring devices were developed in the 1950s,[4–7] specifying the imaging performance of optical components by a modulation transfer function (MTF) became a widely used technique in optical design and quality testing. Although the MTF is commonly used to specify the quality of imaging systems, at present, there is a lack of services offering traceable MTF calibrations.

Motivated by the increasing demand in the industry, the Physikalisch-Technische Bundesanstalt (PTB), in cooperation with an industrial partner, is developing an MTF reference setup for camera lenses with the aim of reaching an expanded measurement uncertainty of 0.01 (coverage probability of 95%) for various measurement configurations. The aims of the project are that an accredited laboratory for MTF calibrations of camera lenses is established and the traceability will be supported by this reference setup.[8]

According to our knowledge, there is currently no commercial MTF measurement setup available offering the desired accuracy for different field heights (on-axis and off-axis).

*Address all correspondence to Melissa Schenker, E-mail: melissa.schenker@ptb.de

Early international comparisons of MTF measurements of lenses have already shown that deviations of several percent between the results of different setups and institutions were typical for the off-axis cases.[9,10] To investigate the present status, in 2018, we performed comparative measurements between different industrial and scientific MTF measurement devices, which have confirmed our assumption that differences of several percent still occur. One of the most critical tasks on MTF test benches regarding measurement uncertainty is the detector positioning, which depends on the alignment procedures and the accuracy of the linear stages moving the detector.

For initially defining the requirements of the mechanical components of our experimental reference setup to meet the desired uncertainty, the influence of misalignments and stage positioning errors on the MTF was estimated separately for every single component. As most of the uncertainty contributions introduced by misalignments and positioning errors depend on the MTF behavior of the lens under test, the measured MTF behavior of typical sample lenses has been considered as well as simulations of the detection process.

However, due to correlations between the effects of different positioning errors on the measured MTF, their combined impact can only be estimated through Monte Carlo studies. We present an optomechanical simulation of our reference setup that considers the misalignments of the source, the collimator, the specimen, and the detector, as well as the positioning errors of the stages moving the detector. This tool may take the uncertainty analysis of MTF measurement setups to a new level, as it gives a fast method of a specimen-specific uncertainty analysis while accounting for the contributions of all misalignments at once and without the need for measured sample lens behavior.

We introduce the working principle and the analysis procedures of the virtual experiments. The main results of the sensitivity analysis of the MTF regarding single parameter variations will be shown together with the combined effects of the mechanical tolerances investigated by Monte Carlo studies. The analysis is carried out for various scenarios that differ in the angle between the optical axis of the setup and the lens under test (on- and off-axis cases). The results of the simulations will be shown for typical sample lenses selected from the projected lens spectrum of the reference setup (see Sec. 2.5).

2 Optomechanical Simulations

The model of the setup is implemented in MATLAB® (MATLAB, 2018) using the software library SimOptDevice[11] developed in the PTB. The software uses object-oriented modeling of the mechanical and optical components combined with optical ray tracing. One advantage of this application over other commercially available optic simulation tools is the definition of separate coordinate systems for the single components of the setup. Due to their arrangement in a hierarchical structure, angular and translational errors of single elements can be implemented straightforward and are applied to all underlying coordinate systems automatically. In addition, the characteristics of the light source and the algorithms needed for the analysis are known in detail and can be controlled individually. Having full control of the software, other influences—e.g., thermal or electronic—can also be implemented, if necessary.

In this section, we consider the working principle and structure of the virtual experiments. After describing the configuration of the setup, the computation of the MTF from the ray-tracing data will be explained. For that, the library of SimOptDevice was complemented by diffraction considerations. Subsequently, the procedure for performing Monte Carlo studies will be introduced together with the three sample lenses for which the analysis will be shown in Sec. 3.

2.1 *Configuration of the Reference Setup*

The MTF reference setup is arranged in a standard infinite–finite configuration following ISO 9335.[12] The model of the setup is shown in Fig. 1. Originating from a point source, the light passes through the collimator and uniformly illuminates the lens under test. The collimator has an aperture of 80 mm and a focal length of 1185 mm. The detector is placed in the image plane of the lens under test by a combination of three linear stages moving in the directions of the x, y, and z axes. In the simulation, the coordinate system is rotated so that the x axis points in the direction of the optical axis, whereas the z axis points in the vertical direction.

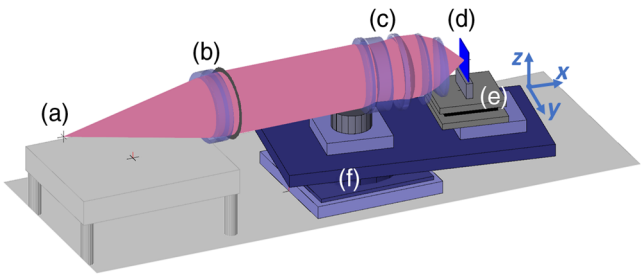

Fig. 1 MTF reference setup in the optomechanical simulation. (a) Point light source, (b) collimator, (c) lens under test, (d) detector plane, (e) three linear stages, and (f) rotary table.

The lens and the detector are arranged on a rotary table to achieve various angles of incidence and field heights. The setup is designed for the visible spectrum, ranging from 400 to 800 nm. In the experiments as well as in the simulations, typically, a wavelength of 546 nm is used.

In the experimental setup, two different detection methods can be applied to measure the intensity distribution on the image plane, from which the MTF is to be calculated. The first one takes one-shot measurements with a combination of a charge-coupled device or complementary metal oxide semiconductor camera and a microscope objective lens, whereas the second is a scanning method consisting of a thin metal slit on a photodetector without the need for relay optics.

To evaluate the influence of the mechanical alignment of the setup independently of the detection method, the detector in the simulation is represented by a simple virtual detection plane. It is placed on the focal plane of the sample lens, which is defined by the highest MTF value at a certain spatial frequency. The calculation of the focal plane position is described in Sec. 2.3.

2.2 *Calculation of the MTF*

For calculating the MTF out of the ray-tracing data, initially, the rays are traced through the complete optical system from the light source to the virtual detector on the image plane. For each ray arriving at the detector, the direction $\vec{e}_{\mathrm{det}}$, the intersection points with the detector plane $\vec{p}_{\mathrm{det}}$, the intensity I_{det}, and the optical path length (OPL) are calculated.

The MTF of the geometric aberrations is estimated by handling the spot diagram as a geometrical point spread function (PSF), from which the one-dimensional (1-D) line spread function (LSF) can be calculated according to the following equation:[13]

$$\mathrm{LSF}(y) = \int_{-\infty}^{\infty} \mathrm{PSF}(y, z)\mathrm{d}z. \tag{1}$$

As the PSF is given through a discrete spot diagram, Eq. (1) cannot be used in the integral form. Instead, an increment dy is defined and all intersection points $\vec{p}_{\mathrm{det}}$ lying between the boundary lines $\pm dy/2$ around the position y are counted and weighted by their intensity to get the LSF. For this geometrical calculation of the LSF, the ray density of the source is chosen so that ~100,000 rays arrive on the detector plane. In the simulations, the interval dy is fixed at a value of 0.1 μm. This corresponds to the smallest effective pixel size that can be currently achieved with our reference setup. The camera used in the setup has a pixel size of 6.5 μm and can be combined with a microscope objective with a magnification of up to 63×. A higher magnification is not compatible with this camera as the effective field of view would be too narrow.

The detector is arranged on the $y - z$ plane, where z defines the vertical direction according to Fig. 1. Therefore, Eq. (1) describes the calculation of the tangential LSF. The sagittal LSF is calculated in the same way by integrating over the y direction. The 1-D geometrical MTF is then calculated by Fourier transformation and is given by[14]

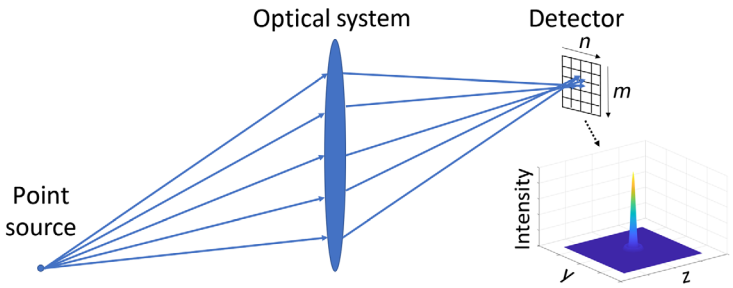

Fig. 2 Principle of the diffraction PSF calculation on the image plane. The rays are traced through the complete optical system. At each point on the detector, the interference of the plane waves assigned to all rays is computed.

$$\mathrm{MTF}(s) = \mathcal{FT}[\mathrm{LSF}(y)]. \tag{2}$$

As the computed MTF only contains information about the geometrical aberrations of the system, it has to be multiplied by the diffraction-limited MTF of the optical system to obtain a reasonable result.[15] The diffraction-limited MTF is a function of the f number of the sample lens and the used wavelength. This fast procedure gives the reliable estimations about the MTF when the geometrical aberrations of the sample lens are large compared with the diffraction limit.

For lenses with a better degree of correction, the MTF relates to the size of the diffraction pattern and, therefore, diffraction effects have to be considered.[16] The method used in the virtual experiments in this case is based on the Huygens principle, where plane wavefronts are assigned to each ray. The intensity distribution on the detector (diffraction PSF) is determined by the interference of the wavefronts on the image plane through superposition. For this purpose, a detector grid of n times m pixels is defined on the image plane perpendicular to the optical axis as shown in Fig. 2.

The positions of the pixels in space $\vec{r}_{n,m}$ depend on the chosen pixel size. At every pixel (indexed by n and m), the complex amplitude sum of all rays j is determined from

$$E(\vec{r}_{n,m}) = \sum_{j=1}^{n_{\mathrm{rays}}} \sqrt{I_{\mathrm{det},j}} \times \exp\left[\frac{2\pi i}{\lambda}\left(\frac{\vec{e}_{\mathrm{det},j}}{|\vec{e}_{\mathrm{det},j}|} \times (\vec{r}_{n,m} - \vec{p}_{\mathrm{det},j}) + \mathrm{OPL}_{\mathrm{det},j}\right)\right], \tag{3}$$

where n_{rays} gives the number of rays arriving at the detector (adapted from Ref. 17). The phase difference of the complex amplitude of a ray j is similar to the absolute OPL of the wavefront covered when reaching the pixel (n, m). It is calculated as the sum of the $\mathrm{OPL}_{\mathrm{det},i}$ at the intersection point $\vec{p}_{\mathrm{det},i}$ and the optical path difference between the plane wave intersecting the detector at $\vec{p}_{\mathrm{det},i}$ and the same plane wave intersecting the detector at $\vec{r}_{n,m}$. The resulting intensity is the modulus squared of the total complex amplitude given by

$$I(\vec{r}) = |E(\vec{r})|^2. \tag{4}$$

The LSF and the 1-D MTF are again calculated following Eqs. (1) and (2). For the calculation of the diffraction MTF, n_{rays} is chosen so that a further increase in the number of rays no longer causes any changes in the resulting MTF. For this purpose, typically $\sim 2^{14}$ rays arrive on the detector plane. In both described methods of MTF calculation, the result must be corrected with the MTF introduced by the effective pixel size of 0.1 μm.

2.3 *Focusing Procedure of the Detector*

To calculate the MTF of the sample lens for an ideally aligned system, the detector has to be placed at the desired focal plane. To get near to that position in the first place, the detector is set to the geometric focal point (GFP) on the optical axis. The GFP is estimated by performing a ray trace from the source to the last surface of the lens under test and subsequently computing the position of the smallest spot size behind the lens in both lateral directions. To stay close to

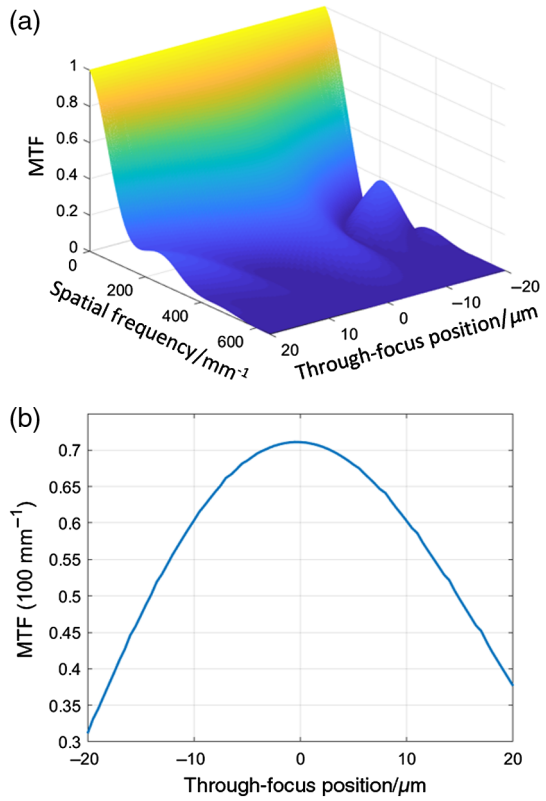

Fig. 3 (a) Exemplary through-focus curves for sample lens 2 (see Sec. 2.5) with a step size of 0.5 μm. (b) The FCP lies at −0.5 μm relative to the GFP.

experimental procedures, a through-focus curve is determined from this point by setting the detector at different points along the optical axis and searching for the position of the highest MTF at a preassigned spatial frequency [focal criterion position (FCP)]. Depending on the properties of the lens under test, the FCP can lie about a couple of microns away from the GFP. An example of a through-focus curve is shown in Fig. 3. With this procedure, we initially align the detector position. However, it has to be mentioned that the calculated FCP can lie about half the step size of the through-focus curve away from the ideal FCP.

2.4 *Sensitivity Analysis*

To investigate the combined effects of the alignment errors on the MTF, Monte Carlo studies are performed. For that, initially, a sample lens has to be included into the simulation. Afterward, a through-focus curve is calculated to determine the MTF of the initially aligned system. Depending on the characteristics of the sample lens, either the geometrical or the Huygens MTF is calculated.

Furthermore, the tolerances of the angular and translational positioning errors of all components of the setup are defined. An overview is shown in Sec. 3.1, where the sensitivity of the MTF on certain misalignments of single elements is also discussed.

Before calculating the MTF of the system for multiple configurations of alignment errors, a closer look has to be taken at the position of the detector during the study. Introducing mechanical deviations into the model may lead to a significant offset of the FCP. In the real experiment, the focusing procedure already includes most of the alignment errors of the system. To keep the simulation close to the experiment, for every configuration of alignment errors, the FCP has to be recalculated and the detector set correspondingly.

When performing a study with ~5000 different configurations of alignment errors, recalculating the FCP each time would lead to a significantly increased computing time. To avoid this procedure when unnecessary, before computing an actual study, a smaller focal point study is

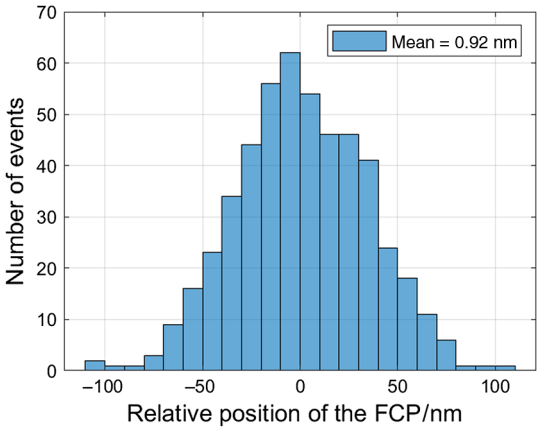

Fig. 4 Exemplary focal point study of sample lens 2 (see Sec. 2.5) for 500 configurations of alignment errors.

carried out to check for significant changes of the FCP. An example of a focal point study is shown in Fig. 4.

The through-focus curves are calculated with an axial step size of 500 nm for 500 different configurations of alignment errors lying in the defined tolerances. The variations of the determined FCPs are of $\sim\pm 100$ nm relative to the FCP determined without alignment errors. The amount of the variations can be explained by deviations of the calculated GFP, resulting in different starting points of the through-focus curves. In contrast, the calculated distance between the FCP and the GFP remains the same for all the configurations.

In this case, the relative position of the FCP to the GFP will only be calculated once in the beginning of the study. During the study, the detector plane will be set to the position resulting from the recalculated GFP and the fixed relative position of the FCP. In addition, random errors with a maximum magnitude of half the step size of the through-focus curves have to be added to the detector position to simulate initial positioning deviations. This agrees with the experiment, as searching for the position of the start point for the through-focus curve is experimentally done by eye and can be assumed to be random in the range of 500 nm. Only setting this start point to the systematically derived GFP each time would ignore this random parameter of the experiment.

In a single Monte Carlo study, ~5000 different configurations of alignment errors are applied and the resulting MTFs are calculated. The deviations of these MTFs to the MTF of the initially aligned system are displayed for certain spatial frequencies in a histogram chart against the number of events. An overview of the complete simulation process is shown in Fig. 5.

2.5 *Sample Lenses*

The reference setup is designed to measure camera lenses with focal lengths in the range of 10 to 135 mm and f numbers between 0.6 and 5. To investigate how the sensitivity and uncertainty estimations depend on the selected specimen, three sample lens designs are selected out of the measurable range to perform exemplary Monte Carlo studies for different measurement configurations.

Sample lens 1 is a telephoto lens with 100 mm focal length and an f number of 1.9 adapted from Ref. 18. The design is well corrected for the on-axis case, but it is only designed for incident angles up to ~2 deg.

Sample lens 2 is a camera lens design with 10 mm focal length and an f number of 2.8 as given in Ref. 19. With a diameter of only a couple of millimeters, this lens represents a miniature wide-angle camera lens. As usual for this lens type, the MTF shows a smooth behavior even at large incident angles.

Sample lens 3 is a simple standard test lens design as described by Williams and Ashton[9] with 50 mm focal length and an f number of 4. This lens is not well corrected but has a simple design, which allows very precise manufacturing. Due to tight tolerances, according to Ref. 9, the manufactured lenses have a maximum expected MTF deviation of ~0.01 MTF units to the computed

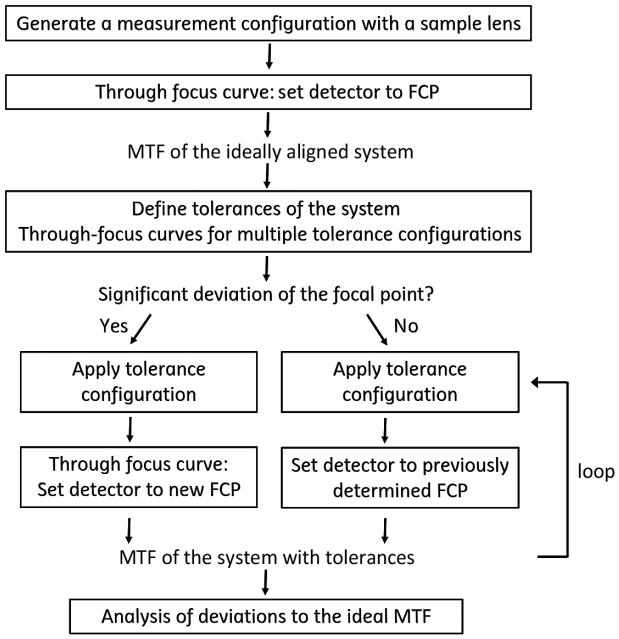

Fig. 5 Tolerancing simulation chart.

design. For this reason, it is a popular sample for testing the performance of an MTF-measuring setup. Williams and Ashton have shown that MTF measurements of the described lens carried out by several laboratories revealed an agreement of better than ± 0.06 MTF units. With the term "MTF unit," we describe the fraction of the maximum MTF value, which is given at a spatial frequency of 0 mm^{-1} where the MTF reaches a value of 1.

3 Results

Some of the main results of the sensitivity analysis of the MTF involving single parameter variations are shown in Sec. 3.1 for sample lens 1. Furthermore, the combined effects of the tolerances are investigated in Secs. 3.2 and 3.3 using Monte Carlo studies for on- and off-axis cases. The on-axis case is defined as the 0-deg position of the rotary table, where the optical axis of the lens under test matches the optical axis determined by the light source and the collimator. In the off-axis case, the angle of the rotary table is different from 0.

3.1 *Sensitivity of the MTF on Certain Parameters*

The positioning errors of the single components studied in the simulations can be divided into the main objects of the setup, which are given by the light source, the collimator, the sample lens, the detector, the rotary table, and the linear stages. For the light source, the axial and lateral deviations from the ideal focal point of the collimator are considered as both of them have an effect on the wavefront behind the collimator. In the simulations, a perfect point light source is assumed so that angular deviations of the source have no influence.

Regarding the collimator, lateral misalignments have the same effect as for the light source. In contrast, an axial deviation is not considered because the absolute distance between the source and the collimator is only aligned once. In addition, the absolute distance between the collimator and the sample lens is of minor importance. For the collimator, the angular deviations (tip and tilt) also have an effect since they introduce wavefront errors.

The sample lens behind the collimator is assumed to be centered to the optical axis with its entrance pupil lying in the rotational axis of the rotary table. Since the incident light cone is highly collimated and has a larger diameter than the entrance pupil, small axial misalignments of the lens are of minor importance. Here, only angular positioning errors are considered. They may be introduced, for example, by a tumbling error of the lens mount.

The detector is placed in the desired focal plane of the sample lens by a combination of three linear stages (XYZ). The positioning errors considered for the detector are a tip and tilt in relation to the plane perpendicular to the optical axis, as well as the axial deviation from the focal plane caused by the quantized steps of the through-focus curves. The amount and distributions of the all positioning tolerances are determined by considerations about the alignment procedures applied to the experimental setup.

The positioning errors of the linear stages are given by the specifications of the manufacturer. The stages are driven by DC motors and are supplied with linear encoders. Errors in the movement of the stages also result in a tip and tilt of the detector and an axial deviation from the desired FCP.

For the air bearing rotary table, the positioning accuracy is determined by the accuracy of the alignment procedure for parallelizing the linear stage in x direction with the optical axis. This value significantly exceeds the specified accuracy of the rotary table itself. The position stability is again given by the provided specifications.

All positioning errors considered in the simulations are listed in Table 1. The errors are assumed to be normally distributed around the ideal positions. One exception is given by the deviation of the detector position from the focal plane in the axial direction. Due to the random start point and the quantized steps of the through-focus curves described in Sec. 2.3, the error is assumed to be equally distributed. The 95% coverage intervals of the alignment errors are given as two times the standard deviations (2σ widths) and are also listed in the table. In addition, the maximum MTF deviations to the tangential MTF of the initially aligned system ($\Delta\mathrm{MTF}_{\mathrm{max}}$) are shown in Table 1 for sample lens 1. The values result from a systematic variation of the single positioning errors in an interval of $\pm 2\sigma$. The calculated $\Delta\mathrm{MTF}_{\mathrm{max}}$ values are given for the on-axis configuration at the spatial frequency of the focal criterion, lying at 100 mm^{-1}. They provide information about the influence of the individual positioning errors on the MTF.

Considering the pitch, roll, and yaw of the three linear stages, a resulting axial shift of the detector position away from the desired focal point has the largest effect on the MTF. Only the corresponding maximum $\Delta\mathrm{MTF}_{\mathrm{max}}$ values are listed in Table 1. For example, with a vertical distance of 95 mm between the x stage and the center of the detector, a pitch of 20 arc sec leads to an axial distance of ~ 9 μm between the detector position and the focal plane. This error gives a maximum MTF deviation of ~ 0.1 MTF units from the MTF of the initially aligned

Table 1 Tolerances included in the simulations and their effect on the MTF (100 mm^{-1}) of sample lens 1.

Object	Positioning error	2σ width	$\Delta\mathrm{MTF}_{\mathrm{max}}$
Light source	Axial deviation	1 mm	1.7×10^{-4}
	Lateral deviation	2 mm	1.4×10^{-3}
Collimator	Lateral deviation	1 mm	1.2×10^{-3}
	Tip/tilt	0.3 deg	4.7×10^{-5}
Sample lens	Tip/tilt	0.01 deg	4.2×10^{-8}
Detector	Axial deviation	250 nm	1.8×10^{-4}
	Tip/tilt	0.1 deg	2.8×10^{-7}
Rotary table	Position accuracy	36 arc sec	7.9×10^{-8}
	Position stability	1 arc sec	2.6×10^{-9}
XYZ linear stages	Position stability	10 to 20 nm	4.8×10^{-6}
	Orthogonality	10 arc sec	—
	Pitch	20 arc sec	9.8×10^{-2}
	Roll/yaw	10 arc sec	1.9×10^{-2}

system at 100 mm^{-1}. This value exceeds the target measurement uncertainty by a factor of 10, but strongly varies for different sample lenses, spatial frequencies, and a different focal criterion or modified measurement instructions. Consequences and potential optimization methods are discussed in Sec. 3.3. In general, the linear stages have to meet high demands in different categories. Especially for a scanning detection method, accurate positioning in the range of 100 nm is required; at the same time, a travel range of several millimeters is needed to reach different image heights. Furthermore, their possible weight is limited due to the placement on a rotary table. Therefore, the stages do not provide the best values regarding the pitch, roll, and yaw as known from precision stages placed on a granite base plate.

In the experiment, the alignment procedures of all components of the setup are performed in the on-axis configuration. This includes the definition of the optical axis, the alignment of the rotary table and the linear stages, and the position of the specimen as well as the detector relative to the optical axis. Therefore, most of the positioning errors resulting from the movement of the linear stages are compensated during alignment. As the linear stages are barely moved in this configuration, the orthogonality of the stages is not relevant and no ΔMTF_{max} value is given in Table 1.

In addition to the positioning errors of the linear stages, the next largest MTF errors are induced by lateral deviations of the light source and the collimator. In this special case, the other positioning errors are of minor importance regarding the ΔMTF_{max} values. Nevertheless, for different sample lenses, spatial frequencies, or measurement instructions, the values may differ significantly. Therefore, all the mentioned positioning errors are included in the simulations.

3.2 *On-Axis Behavior*

In the on-axis case, the optical axis of the sample lens matches the optical axis of the setup. For each sample lens, 5000 configurations of random positioning errors are applied to the setup. The errors lie within the defined tolerances listed in Table 1 and are drawn from a standardized normal distribution. The only exception is given by the axial deviation of the detector position from the focal plane, which is assumed to be equally distributed. For the linear stages, the pitch, roll, and yaw are not applied in the on-axis configuration because of the alignment procedures mentioned in Sec. 3.1. Residual positioning errors resulting from an inclination of the linear stages are considered by directly assigning angular deviations (tip/tilt) and axial positioning errors to the detector.

The focusing procedures are carried out with a step size of 500 nm for each sample lens. In the procedures, the position with the best MTF at 100 mm^{-1} is determined for sample lenses 1 and 2, whereas the best MTF at 20 mm^{-1} is determined for sample lens 3. The resulting MTFs of the initially aligned systems are shown in Fig. 6(a). In Fig. 6(b), the deviations of the MTF to the MTF of the initially aligned system (ΔMTF) are shown for 5000 different configurations of alignment errors for sample lens 1. The results for sample lenses 2 and 3 are displayed in Figs. 6(c) and 6(d), respectively. In these histogram plots, for each sample lens, the results for three exemplary spatial frequencies are displayed.

Comparing the results of the three sample lenses, it can be observed that the maximum ΔMTF values are in the same order of magnitude, and the distributions differ significantly. For sample lens 1, the MTF deviations show a normally distributed behavior, whereas for sample lens 2, they are almost equally distributed. For sample lens 3, the behavior lies somewhere between normal and equal distribution. In addition, sample lens 3 is the only one for which the mean values of ΔMTF differ considerably from each other for the different spatial frequencies. This behavior will be discussed later in this section. The comparison of the three different sample lenses gives an impression on the strong dependence of the measurement uncertainty on the lens to be measured.

For the defined test conditions, within a 95% coverage interval, the MTF deviations from the initially aligned systems are not expected to exceed a value of ~0.004 MTF units. However, aiming an uncertainty of 0.01 MTF units in total, this value already represents a significant contribution to the overall measurement uncertainty. Therefore, the parameters with the biggest impact on the ΔMTF behavior must be identified.

The only equally distributed alignment error applied to the system is given by the start point of the through-focus curves. This is motivated by the missing alignment of the start point of the

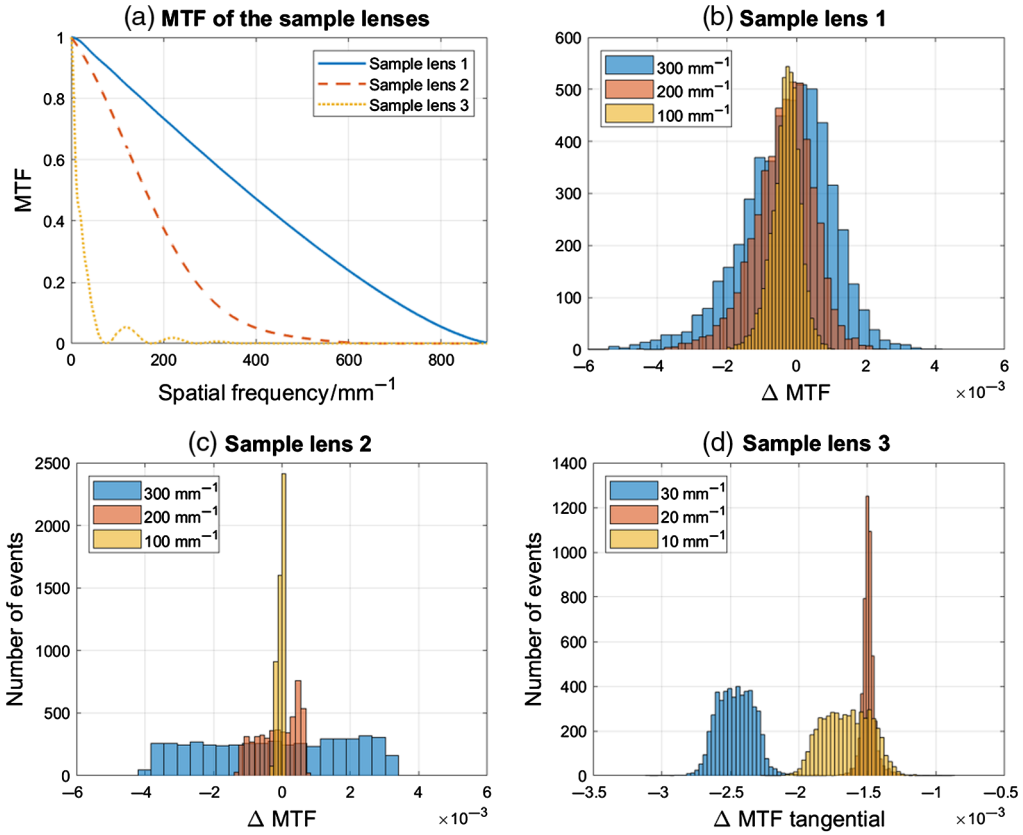

Fig. 6 (a) Behavior of the tangential MTF of each sample lens for the initially aligned systems. The Monte Carlo studies of ΔMTF (tangential) are shown for 5000 configurations for (b) sample lens 1, (c) sample lens 2, and (d) sample lens 3. The step size of the through-focus curves is 500 nm.

through-focus curves, as mentioned in Sec. 2.4. Therefore, the equally distributed behavior shown for sample lens 2 in Fig. 6(c) indicates a strong dependence of the MTF of this sample lens on the axial position of the detector, especially for higher spatial frequencies.

To confirm this assumption, separate investigations into the effect of an axial shift of the detector are carried out for sample lenses 1 and 2. For this purpose, the detector position is varied systematically $\sim \pm 500$ nm relative to the FCP calculated in the focusing procedure, whereas all other alignment errors are set to 0. The range is chosen according to the step size of the through-focus curves. The resulting ΔMTF curves are shown in Fig. 7.

Since the focal criterion lies at 100 mm^{-1} for both sample lenses, the MTF at this spatial frequency gives a maximum response near the calculated FCP and therefore a minimum rate of change. For the other spatial frequencies, the rate of change in the MTF is considerably higher. For sample lens 1, the axial positions of the maximum MTF at 200 and 300 mm^{-1} lie in the displayed range of the relative axial detector position. In the same range, the MTF of sample lens 2 shows an almost linear behavior at 300 mm^{-1}. In addition, in this range, the peak-to-valley value of ΔMTF at 300 mm^{-1} is about three times higher for sample lens 2 than for sample lens 1. These results agree with the assumption of a higher MTF dependence of sample lens 2 on the axial detector position relative to the FCP.

Furthermore, this analysis provides information about the fact that ΔMTF values >0 may occur while misalignments are introduced to the setup. Especially for spatial frequencies other than the one specified for the focal criterion, displacements of the axial detector position away from the FCP may lead to higher MTF values. In addition, for the spatial frequency of the focal criterion, the perfect FCP can lie about half the step size away from the FCP calculated in the through-focus curve. Besides, the alignment of the distance between the source and the collimator can have a similar effect on the resulting MTF.

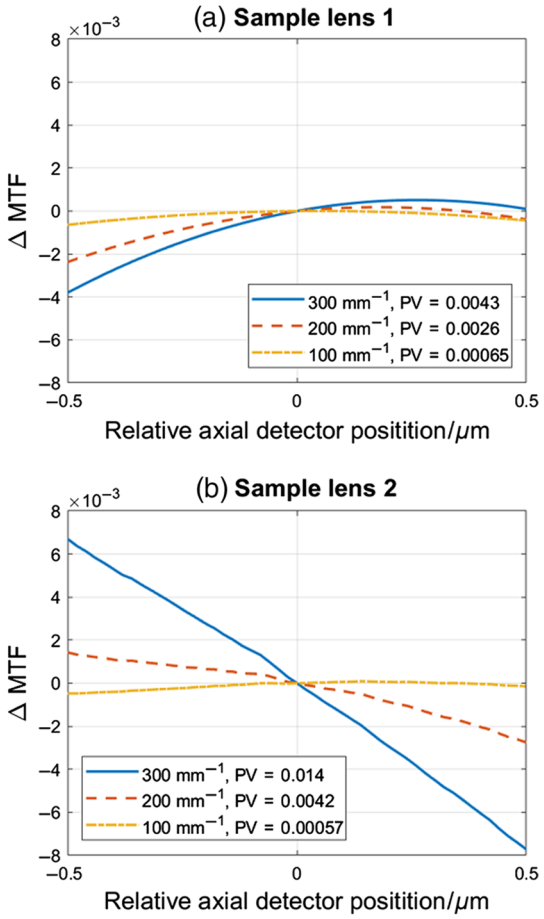

Fig. 7 Behavior of the deviation ΔMTF depending on the axial position of the detector relative to the FCP for (a) sample lens 1 and (b) sample lens 2.

To narrow down the error given by the random start point, the step size of the through-focus curves was reduced by half to 250 nm and again Monte Carlo studies were carried out for all sample lenses. The results for sample lenses 1 and 2 are shown in Fig. 8. It can directly be seen that for sample lens 2 the maximum ΔMTF value at 300 mm^{-1} decreased by almost a factor of two as well. In contrast, adapting the same step size for sample lens 1 only has a small effect on the MTF response. Here, especially, the positioning errors of the source and the collimator have a greater influence than for sample lens 2.

The calculated mean values and 2σ widths of the distributions of ΔMTF are listed in Table 2, depending on the sample lens, the spatial frequency, and the step size of the through-focus curves. For sample lens 3, the smaller step size has almost no influence on the mean values of ΔMTF for the spatial frequencies displayed in Fig. 6(d). However, the distributions of ΔMTF become narrower for the spatial frequencies 10 and 30 mm^{-1} and the equally distributed part of the ΔMTF distributions can almost be eliminated. This can again be explained by an almost linear behavior of the MTF depending on the axial detector position for these spatial frequencies. However, in this case, due to their higher absolute values, the mean values have a greater impact on the overall uncertainty than the 2σ widths of the distribution itself. For this lens, the sensitivity on lateral misalignments and angular displacements is much higher compared with sample lenses 1 and 2. The positive effects on the MTF, which may result from an axial detector shift or also an axial shift of the source, cannot compensate for the combined negative effects on the MTF resulting from the other alignment errors of the setup. Furthermore, it is important to mention that the ΔMTF distributions would change when applying a different focal criterion.

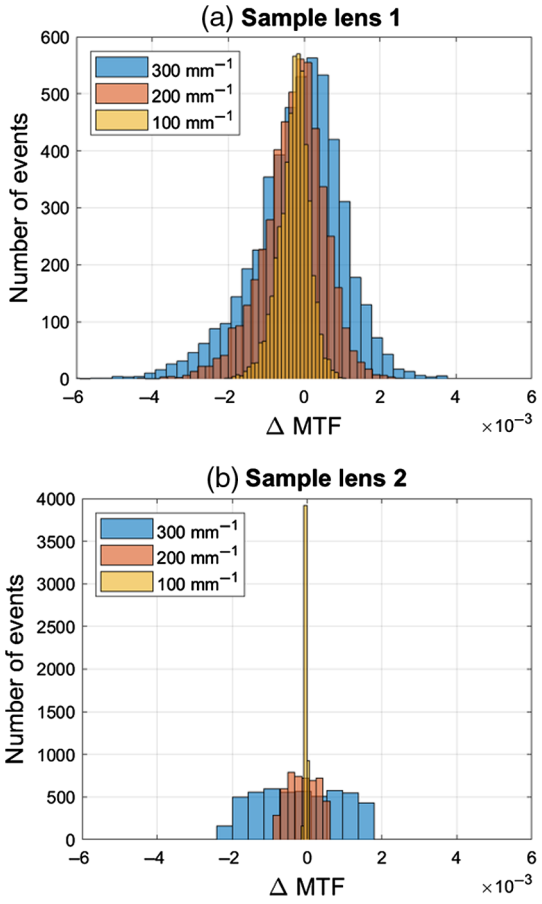

Fig. 8 Monte Carlo studies of ΔMTF (tangential) for 5000 configurations at three exemplary spatial frequencies for (a) sample lens 1 and (b) sample lens 2. The step size of the through-focus curves is 250 nm.

Table 2 Mean and 2σ interval of the on-axis tangential MTF deviation, depending on the sample lens, and the step size of the through-focus curves.

Sample lens	Step size (nm)	100 mm^{-1}		200 mm^{-1}		300 mm^{-1}	
		Mean	2σ	Mean	2σ	Mean	2σ
1	500	-0.30×10^{-3}	0.82×10^{-3}	-0.36×10^{-3}	1.72×10^{-3}	-0.27×10^{-3}	2.55×10^{-3}
	250	-0.27×10^{-3}	0.81×10^{-3}	-0.28×10^{-3}	1.64×10^{-3}	-0.16×10^{-3}	2.35×10^{-3}
2	500	-0.04×10^{-3}	0.17×10^{-3}	-0.13×10^{-3}	1.15×10^{-3}	-0.20×10^{-3}	4.18×10^{-3}
	250	-0.03×10^{-3}	0.05×10^{-3}	-0.11×10^{-3}	0.67×10^{-3}	-0.19×10^{-3}	2.18×10^{-3}
		10 mm^{-1}		20 mm^{-1}		30 mm^{-1}	
3	500	-1.65×10^{-3}	0.34×10^{-3}	-1.49×10^{-3}	0.10×10^{-3}	-2.46×10^{-3}	0.27×10^{-3}
	250	-1.64×10^{-3}	0.15×10^{-3}	-1.49×10^{-3}	0.10×10^{-3}	-2.45×10^{-3}	0.15×10^{-3}

3.3 *Off-Axis Behavior*

The off-axis configurations are adjusted by changing the angle of the rotary table, resulting in a varied incident angle of the light path on the sample lens. To measure the intensity distribution in the desired focal plane, the positions of the linear stages have to be adapted to the corresponding position of the focal point.

The Monte Carlo studies for the off-axis configuration are carried out for sample lens 2, which shows smooth MTF curves even for greater incident angles. Again, random alignment errors lying in the defined tolerances (see Table 1) are applied to the setup. In contrast to the studies performed on-axis, the off-axis studies also consider the pitch, roll, and yaw errors of the linear stages, as well as their orthogonality. The results for the tangential MTF at an incident angle of 5 deg are shown in Fig. 9. It can be seen that the maximum ΔMTF values are considerably higher in this off-axis configuration than in the on-axis configuration as shown in Fig. 6(c). While aspiring to a measurement uncertainty of 0.01, in this configuration, the maximum ΔMTF value lies at 0.357 MTF units for a spatial frequency of 100 mm^{-1}. The big differences to the on-axis case can be explained by the defined off-axis measuring instructions and the errors induced by the motion of the linear stages.

Regarding the application of camera lenses, the distance between the plane image sensor and the lens is fixed during image acquisition. Therefore, typical MTF-measuring instructions demand that the distance between the sample lens and the detector is the same in the off-axis case as for the FCP determined in the on-axis case. Assuming that the linear stages are ideally aligned, only the position of the y axis has to be adjusted to the corresponding field height for the off-axis configuration.

In practice, the pitch, roll, and yaw of the linear stages and their nonperfect orthogonality result in differences between the detector position and the desired focal plane. Here, the strongest influence on the MTF is exerted by deviations of the detector position in the direction of the x axis (parallel to the optical axis), as already mentioned in Sec. 3.1. The pitch of the x stage, for example, results in a maximum detector shift of ∼9 μm in x direction. In this context, the

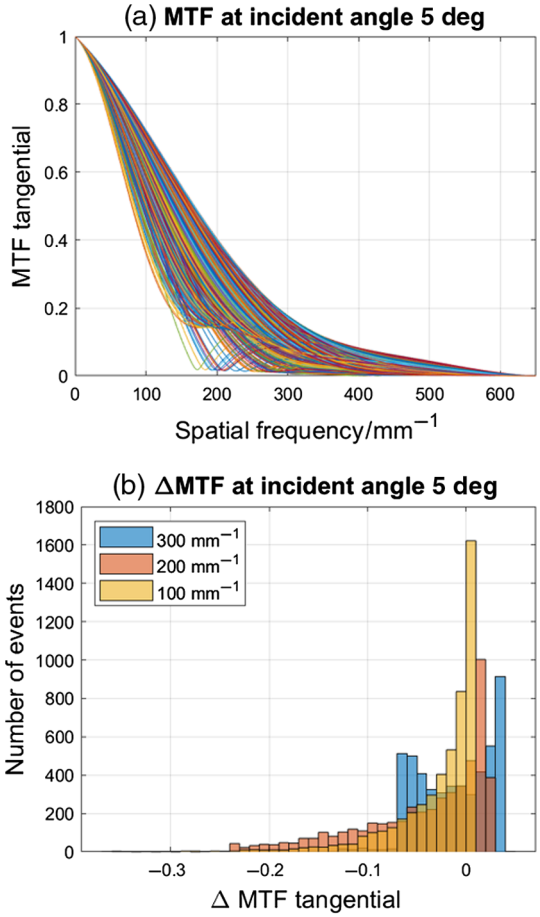

Fig. 9 Off-axis Monte Carlo studies of sample lens 2 without axial correction of the detector position. (a) Tangential MTFs for 5000 configurations. (b) Deviation of the tangential MTFs from the initially aligned system.

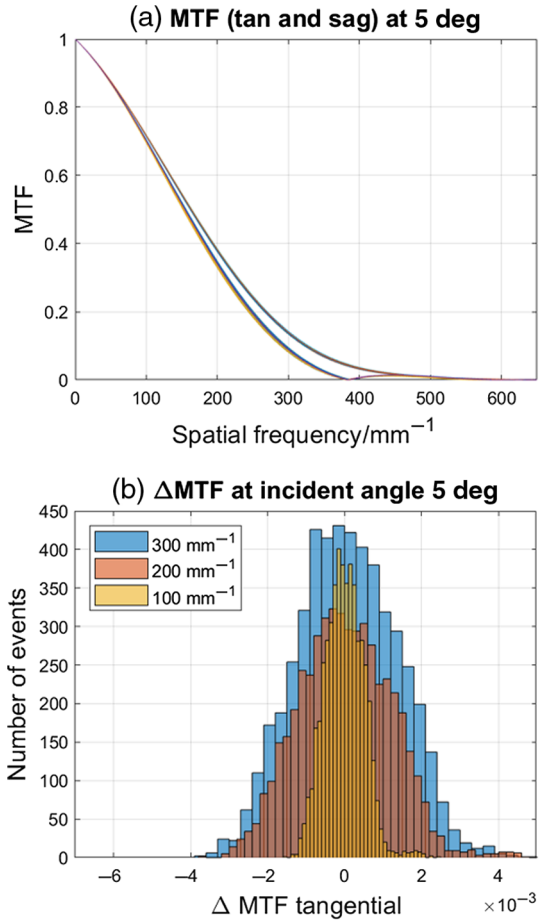

Fig. 10 Off-axis Monte Carlo studies of sample lens 2 with axial correction of the detector position. (a) Tangential and sagittal MTFs for 5000 configurations. (b) Deviation of the tangential MTFs from the initially aligned system.

orthogonality of the linear stages only plays a minor role. At a field height of 0.87 mm, corresponding to the incident angle of 5 deg, the maximum orthogonality error of 10 arc sec leads to a shift in the detector position of ∼40 nm in the direction of the x axis.

To prove that the main error of the MTF is induced by the shift of the detector in x direction, the same studies are carried out again by additionally correcting the axial detector position in the direction of the x axis after adjusting the linear stages. The results of the tangential and the sagittal MTF are shown in Fig. 10. By applying this corrective procedure, the maximum ΔMTF value at 100 mm^{-1} is reduced from 0.357 to 0.0024 MTF units.

The off-axis studies for sample lens 2 are carried out at three different incident angles for 5000 configurations each. The results are listed in Table 3 and they include the maximum deviation of the tangential and sagittal MTF from the initially aligned system (ΔMTF_{max}) for three different spatial frequencies. Additionally, all studies are calculated with and without the correction of the detector position in the direction of the x axis. A comparison of the two methods can also be found in Table 3. It can be seen that this correction procedure reduced the maximum ΔMTF values up to a factor of ∼600.

4 Discussion

The results of the virtual experiments confirm the assumption that the positioning of the detector in the desired focal plane is one of the most critical parts in MTF test benches. The on-axis cases demonstrate that, depending on the lens under test, an adaption of the step size in the focusing

Table 3 Results of the maximum ΔMTF values for sample lens 2 at three different incident angles.

		ΔMTF_{max} 100 mm^{-1}		ΔMTF_{max} 200 mm^{-1}		ΔMTF_{max} 300 mm^{-1}	
Angle	Correction	Tan	Sag	Tan	Sag	Tan	Sag
2 deg	No	0.338	0.336	0.361	0.357	0.130	0.131
	Yes	0.0006	0.0020	0.0023	0.0055	0.0046	0.0071
5 deg	No	0.357	0.419	0.362	0.304	0.130	0.118
	Yes	0.0024	0.0050	0.0057	0.0108	0.0056	0.0086
10 deg	No	0.289	0.468	0.379	0.438	0.222	0.187
	Yes	0.0039	0.0170	0.0019	0.0118	0.0050	0.0047

procedure can reduce the uncertainty contributions significantly. For the off-axis cases, the results show a critical influence of the travel errors of the linear stages resulting in a deviation of the detector position away from the desired focal plane. These errors have to be compensated by corrective procedures to achieve acceptable uncertainty contributions.

Two basic procedures can be applied to reduce the influence of stage imperfections. One is to adjust the orthogonality based on symmetry checks. If no mechanical adjustments are possible, these can be applied in the positioning software. The other is to apply an additional position measuring system and use the data for the positioning. As far as the positioning stages show reproducible errors, the system can be calibrated for these.

As an additional position measuring system, interferometric length measurements in combination with reference mirrors placed on the linear axes could be used. Alternatively, laser tracer systems can be used, which are well known for the calibration of coordinate measuring machines.[20]

These coordinate measurement calibration procedures are not yet considered in the present simulations since the intention was to investigate the basic effects and show the demands on the positioning. To achieve an uncertainty of 0.01 MTF units, simulations have shown that an accuracy of the axial detector position in the range of the step size of the through-focus curve (250 nm) seems to be sufficient for sample lens 2.

In applying the mentioned corrective methods, care must be taken to ensure the necessary precision. Especially, the pitch, roll, and yaw of the stages may also have statistical components whose amount varies with different stage types. For a desired accuracy in the submicrometer range, a constant and direct measurement of the distance between the lens under test and the detector by an additional position measuring system can provide a traceable method.

Some minor aspects have not yet been considered in the simulations, i.e., temperature effects, inhomogeneities of the refractive index in the optical components and the air, surface irregularities of the optics, the bandwidth of the wavelength, or scattered light in the lens under test. Therefore, the simulations do not provide exact information about the absolute MTF values of specific lenses, as they would be measured in the experimental setup. Nevertheless, the simulations allow estimations about the magnitude of the MTF errors induced by mechanical misalignments. Thereby, they are a useful tool to assess whether the mechanical tolerances of the system satisfy the requirements and, if needed, to find constructive optimization strategies.

Furthermore, the big differences in the ΔMTF behavior of the different sample lenses demonstrate the complexity of assigning a specific uncertainty to an MTF-measuring setup. At least for uncertainties ~0.01 MTF units, a high dependence is observed on the lens to be measured, the desired spatial frequency, the chosen focal criterion, and the specified test conditions. However, in most of the discussed scenarios, the maximum MTF deviations are well below the target measurement uncertainty of 0.01 MTF units. Therefore, considering only the errors induced by the mechanical alignment, it can be assumed that the desired measurement uncertainty may be achieved.

5 Conclusions

We implemented our MTF reference setup in an optomechanical simulation environment, which is capable of performing virtual experiments under realistic measuring instructions. The sensitivity of the MTF measurements on positioning errors of the light source, the collimator, the lens under test, the detector, and the stages has been investigated by varying single tolerancing parameters, and the combined effects of all possible misalignments have been analyzed within Monte Carlo studies.

The virtual experiments present a progressive tool for a fast and lens-specific analysis of the overall measurement uncertainty induced by the mechanical alignment in an MTF measurement setup. The simulations provide a deeper insight into the MTF behavior of different sample lenses and help to find constructive optimization strategies. Especially, the results sensitize for the necessary precision of the detector position, which may lie in the submicrometer range for high-precision MTF measurements. Using the mentioned optimization strategies, the results indicate that the desired measurement uncertainty of 0.01 MTF units may be achieved in our reference setup.

In the next step, the verification of the simulation results by experimental investigations is proposed. Furthermore, the optomechanical virtual experiments are to be combined with simulations of the detection methods to come closer to a holistic simulation of the measurement process.

Acknowledgments

The funding of the project by the TransMeT program of the German Federal Ministry for Economic Affairs is gratefully acknowledged. The authors declare no conflicts of interest.

References

1. D. W. Hertel and E. Chang, "Image quality standards in automotive vision applications," in *IEEE Intell. Veh. Symp.*, pp. 404–409 (2007).
2. D. Reshidko and J. Sasian, "Optical analysis of miniature lenses with curved imaging surfaces," *Appl. Opt.* **54**(28), E216–E223 (2015).
3. F. E. Sahin, "Long-range, high-resolution camera optical design for assisted and autonomous driving," *Photonics* **6**(2), 73 (2019).
4. E. H. Linfoot, "Information theory and optical images," *J. Opt. Soc. Am.* **45**(10), 808–819 (1955).
5. H. H. Hopkins, "On the diffraction theory of optical images," *Proc. R. Soc. A* **217**(1130), 408–432 (1953).
6. H. H. Hopkins, "The application of frequency response techniques in optics," *Proc. Phys. Soc.* **79**(5), 889–919 (1962).
7. K. Rosenhauer and K. J. Rosenbruch, "Ein Verfahren Zur Messung der Kontrast-Übertragungsfunktion Photographischer Objektive," *Opt. Acta: Int. J. Opt.* **4**(1), 21–30 (1957).
8. M. Schenker et al., "Development of a high-precision MTF reference setup," in *Proc. Eur. Opt. Soc. Biennial Meeting*, pp. 494–495 (2018).
9. T. L. Williams and A. Ashton, "The use of standard test lenses for verifying the accuracy of OTF equipment," *Appl. Opt.* **8**(10), 2007–2012 (1969).
10. Commission of the European Communities, "Optical transfer function measurement intercomparison, BCR information applied metrology," EUR 11773 EN (Synopsis report prepared by K. G. Birch) (1988).
11. R. Schachtschneider et al., "SimOptDevice: a library for virtual optical experiments," *J. Sens. Sens. Syst.* **8**(1), 105–110 (2019).
12. International Organization for Standardization, "Optics and optical instruments. Optical transfer function. Principles and procedures of measurement," ISO 9335, Geneva, Switzerland (1995).

13. T. Williams, *The Optical Transfer Function of Imaging Systems*, Routledge, New York (1999).
14. J. D. Gaskill, *Linear Systems, Fourier Transforms, and Optics*, Wiley, New York (1978).
15. G. D. Boreman, *Modulation Transfer Function in Optical and Electro-Optical Systems*, SPIE Press, Bellingham, Washington (2001).
16. W. J. Smith, *Modern Optical Engineering*, McGraw-Hill, New York (2008).
17. M. Born and E. Wolf, *Principles of Optics: Electromagnetic Theory of Propagation, Interference and Diffraction of Light*, Elsevier, Amsterdam (2013).
18. ZEMAX®, *Zebase 6. Optical Design Database*, p. 115, Radiant ZEMAX, LLC, Bellevue, Washington (2011).
19. M. Laikin, *Lens Design*, 4th ed., p. 70, CRC Press, Boca Raton, Florida (2012).
20. J. Sladek et al., "Virtual coordinate measuring machine built using lasertracer system and spherical standard," *Metrol. Meas. Syst.* **20**(1), 77–86 (2013).

Biographies of the authors are not available.